Electrochimica Acta 164 (2015) 38–47

Contents lists available at ScienceDirect

Electrochimica Acta

journal homepage: www.elsevier.com/locate/electacta

Effects of interface modification with self-assembled monolayers on the photovoltaic performance of CdS quantum dots sensitized solar cells

Lili Yang [a], Gang Chen [a], Yunfei Sun [a], Donglai Han [b,c], Shuo Yang [b,c], Ming Gao [a], Ping Zou [a], Hongmei Luan [a], Xiangwang Kong [a], Jinghai Yang [a,*]

[a] Key Laboratory of Functional Materials Physics and Chemistry of the Ministry of Education, Jilin Normal University, Siping 136000, Jilin, China
[b] State Key Laboratory of Luminescence and Applications, Changchun Institute of Optics, Fine Mechanics and Physics, Chinese Academy of Sciences, Changchun 130033, China
[c] University of Chinese Academy of Sciences, Beijing 100049, China

ARTICLE INFO

Article history:
Received 14 September 2014
Received in revised form 16 January 2015
Accepted 23 February 2015
Available online 24 February 2015

Keywords:
Self-assembled monolayers
Work function
Surface defects

ABSTRACT

We employ 3-PPA, BPA and APPA as self-assembled monolayers (SAMs), who owns the same phosphonic acid headgroup but different tail group, to modify the surface of ZnO nanorods. Their effects on the photovoltaic performance of quantum dots sensitized soar cells are systematically investigated. The results indicate that the deposition of SAMs not only passivates the surface defects of ZnO nanorods, but also tunes their surface work function to adjust the band alignment of solar cells. In particular, the 3-PPA modification exhibits the best passivation effect and makes the surface work function of ZnO decreases by 1.04 eV to realize a better band alignment due to its electron-withdrawing tailgroup, which results in an enhancement in photovoltaic conversion efficiency of solar cells.

1. Introduction

Quantum dots sensitized solar cells (QDSSCs) as a derivative for dye-sensitized solar cells (DSSCs) attract lots of attention in recent years. However, its power conversion efficiency is much lower than 13% of DSSCs [1,2]. The back electron transfer and recombination processes of photogenerated carriers at the interface are known to be the main factors for such lower efficiency of QDSSCs. Therefore, how to prevent the back electron transfer or recombination processes and accelerate the transportation of separated charge to the contact electrode is an effective way to improve the efficiency of QDSSCs.

Self-assembled monolayers (SAMs) of organic molecules are two-dimensional molecular arrays formed spontaneously on a solid inorganic surface by adsorption [3]. The SAMs consists of three groups: a head group that enables the molecule to anchor to a surface, a carbon backbone chain whose length significantly influences the packing density of the SAMs [4,5], and a tail group that determines interfacial properties of the SAMs [6–9].

As surface modifiers, the SAMs such as silanes [10], amines [11–13], thiols [14–16], carboxylic acids [17–23], and phosphonic acids [24–26] are widely used in the photoelectric devices to improve the performance. Among these groups, the phosphonic acids attract our attention, since they can not only robustly bind on the metal oxide surfaces by relatively simple process, but also form more homogeneous surface with a lower surface energy and better interfacial compatibility with organic overlayers [27].

The phosphonic acids molecules have been used to modify the surface of ZnO [24,25,28]. Perkins et al. [28] chose the SAMs of hexylphosphonic acid and hexanethiol to modify the surface of ZnO and found that the SAMs with phosphonic acid headgroups provide the stronger attachment to ZnO. Hence, in this work, we employed three organic molecules with phosphonic acid headgroup but different tail group as SAMs to modify the surface of ZnO nanorods (NRs), i.e. 3-Phosphonopropionic acid (3-PPA), Butylphosphonic acid (BPA) and 3-Aminopropylphosphonic acid (APPA). These SAMs/ZnO NRs were used as photoanodes to fabricate CdS QDs sensitized solar cells. Fig. 1 illustrates the schematic structure of QDSSCs and the molecule formulas of SAMs. Comparing their molecule formula, we can see that the electron-withdrawing and electron-donating functions of their tail groups are different, so that their effects on the ZnO surfaces and photovoltaic performance of solar cells will be different. In particular, we utilized

* Corresponding author at: Department of Physics, Jilin Normal University, Siping 136000, China. Tel.: +86 434 3294566; fax: +86 434 3294566.
E-mail addresses: llyang@jlnu.edu.cn (L. Yang), jhyang1@jlnu.edu.cn (J. Yang).

http://dx.doi.org/10.1016/j.electacta.2015.02.190
0013-4686/

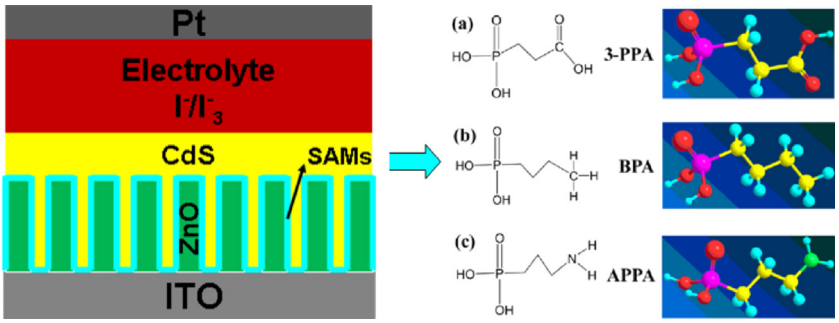

Fig. 1. Device architecture of the QDs solar cell with SAMs modified ZnO. The molecule formula of three difference SAMs, (a) the 3-PPA, (b) the BPA, (c) the APPA. The O, P, C, N and H atoms are presented by the red, magenta, yellow, green and light blue color, respectively. (For interpretation of the references to color in this figure legend, the reader is referred to the web version of this article.)

ultraviolet photoelectron spectroscopy (UPS) to investigate three SAMs on the work function of ZnO surface, so that their effects on the photovoltaic performance of solar cells can be revealed.

2. Experimental

2.1. Preparation of vertically aligned ZnO NRs

The indium tin oxide (ITO) substrates were ultrasonic cleaned in acetone, alcohol and deionized water for 15 minutes in sequence. All chemicals (analytical grade reagents) were directly used without further purification. The ZnO NRs arrays were grown on ITO substrates by two-step chemical bath deposition (CBD) method, including a substrate treatment prior to the CBD growth. The detailed process can be found in our previous report [29–31]. In this case, ZnO NRs arrays were grown in the chemical solution for 6 h under 95 °C.

2.2. Deposition of SAMs: 3-PPA, BPA, APPA

To realize the effective deposition of SAMs, three ZnO NRs samples were separately dipped into 10 mM 3-PPA ethanol solutions, 10 mM BPA ethanol solutions and 10 mM APPA ethanol solutions for 1 min. After immersion, they were rinsed with ethanol to remove excess molecules. These samples were named as 3-PPA(1 min)/ZnO, BPA(1 min)/ZnO and APPA(1 min)/ZnO, respectively. Here we would like to mention two things. On one hand, the formation and properties of SAMs on the surface of solids are generally sensitive to the pH of the solution. In our case, the native pH of 3-PPA(10 mM), BPA(10 mM), APPA(10 mM) ethanol solution is ~2.5, ~3.2, ~5.4, respectively. To determine the unified pH value for these three ethanol solution, we adjusted the pH of 3-PPA ethanol solution from 2.5 to 3.2 and 5.4 by the concentrated ammonia and investigated its effects on the photovoltaic performance of QDSSCs. The results showed that the solar cell exhibits the highest conversion efficiency when pH is 5.4 (See Fig. S1 in Supporting Information). Therefore, all three SAMs were deposited on the ZnO NRs with adjusting pH to 5.4. On the other hand, we also investigated the effects of the concentration of 3-PPA ethanol solution (1 mM, 10 mM, 100 mM) and immersion time (30 s~72 h) on the photovoltaic performance of QDSSCs (See Fig. S2 and Fig. S3 in Supporting Information). When the 3-PPA concentration is 10 mM and deposition time is 1 min, the solar cell exhibits the best photovoltaic performance.

2.3. Deposition of CdS QDs

The CdS QDs were in-situ deposited on the surfaces of SAMs/ZnO and pure ZnO NRs by a successive ionic layer adsorption and reaction (SILAR) technique [32]. To complete a SILAR cycle, the ZnO samples were first immersed into $Cd(NO_2)_2$ (0.1 M) solution for 5 min. They were then rinsed with deionized water for 30 s to remove excess ions weakly bound to the surface of samples and then immersed in a Na_2S (0.1 M) solution for another 5 min followed by another rinsing with deionized water. These SILAR cycles were repeated about 20 times. Subsequently, the samples were thoroughly washed with ethanol and deionized water and then dried at room temperature for fabricating solar cells.

2.4. Cell fabrication

The photoelectrode consisting of CdS/SAMs/ZnO was incorporated into thin layer sandwich-type cells. A 20 nm platinum-sputtered ITO substrate as the counter electrode and the working electrode were positioned face-to-face. The iodide-based electrolyte, consisting of 1 M LiI and 0.05 M I_2 in alcohol, was injected into the interelectrode space by capillary action.

2.5. Characterization and measurements

The X-ray diffraction (XRD) patterns were recorded by a MAC Science MXP-18 X-ray diffractometer using a Cu target radiation

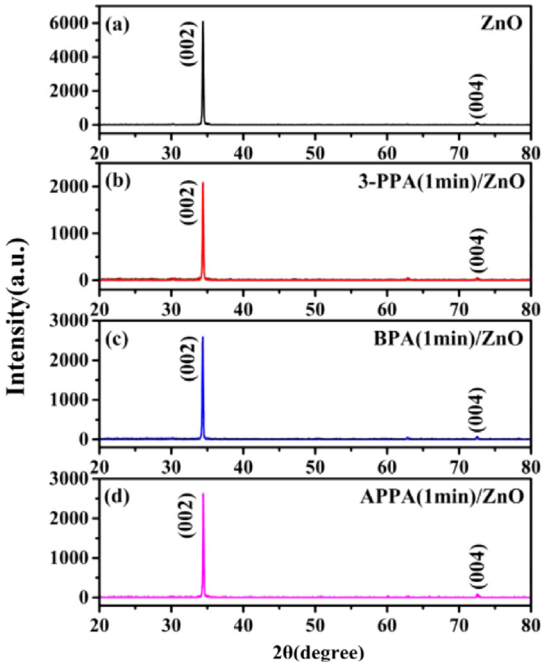

Fig. 2. XRD patterns of the ZnO NRs (a), 3-PPA(1 min)/ZnO (b), BPA(1 min)/ZnO (c) and APPA(1 min)/ZnO (d).

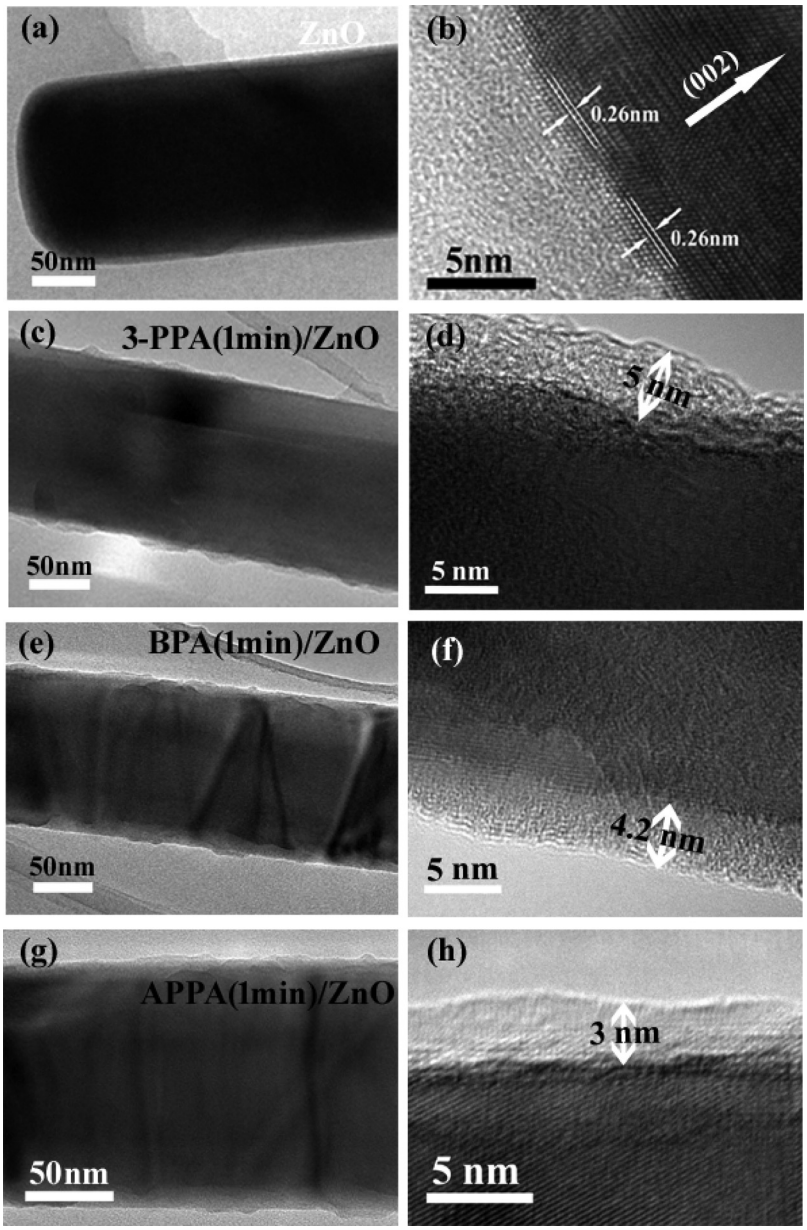

Fig. 3. TEM images of ZnO NRs (a), 3-PPA(1 min)/ZnO (c), BPA(1 min)/ZnO (e) and APPA(1 min)/ZnO (g), and HRTEM images of ZnO NRs (b), 3-PPA(1 min)/ZnO (d), BPA(1 min)/ZnO (f) and APPA(1 min)/ZnO (h).

source. The transmission electron micrographs (TEM) and high-resolution transmission electron microscopy (HRTEM) images were taken on JEM-2100 transmission electron microscope. X-ray photoelectron spectra (XPS) were recorded on a VG ESCALAB Mark II XPS using Mg Kα radiation ($h\upsilon = 1253.6$ eV) with a resolution of 1.0 eV. Fourier transform infrared (FTIR) spectrum was recorded on a Bruker Vertex 70 spectrophotometer in KBr pellets. Water contact angle measurements were performed by contact angle analyzer (Phoenix 300, SEO) at room temperature (RT). The Ultraviolet–Visible (UV–Vis) absorption spectra of each photoelectrode were recorded on a UV–vis spectrophotometer (UV-5800PC, Shanghai Metash Instruments Co., Ltd.) at room temperature. The photoluminescence (PL) measurements were performed on the Renishaw invia spectroscopy excited by a continuous He–Cd laser with a wavelength of 325 nm at a power of 2 mW. The performance of ultraviolet photoemission spectroscopy (UPS) was carried out with a helium discharge lamp ($h\nu = 21.22$ eV) in normal emission with a sample bias of −8 V. The photocurrent dependence on the voltage (I–V) were measured under AM 1.5 G simulated sunlight illumination (100 mW/cm^2, Model 91160, Oriel).

3. Results and discussions

Fig. 2 illustrates the XRD patterns of the as-grown ZnO NRs, 3-PPA(1 min)/ZnO, BPA(1 min)/ZnO and APPA(1 min)/ZnO. For all four patterns, we can only observe two diffraction peaks, which can be indexed to ZnO with hexagonal wurtzite structure according to the JCPDS card (No. 80-0074). These phenomena indicate that ZnO NRs in four samples are preferentially oriented in the c-axis direction [33]. Moreover, as compared to the XRD pattern of ZnO NRs, the intensities of (0 0 2) diffraction peaks for SAMs(1 min)/ZnO turn weak, which maybe due to the surface modification of SAMs.

To reveal the morphology variation after depositing SAMs, the detailed microscopic structure of ZnO NRs and SAMs(1 min)/ZnO

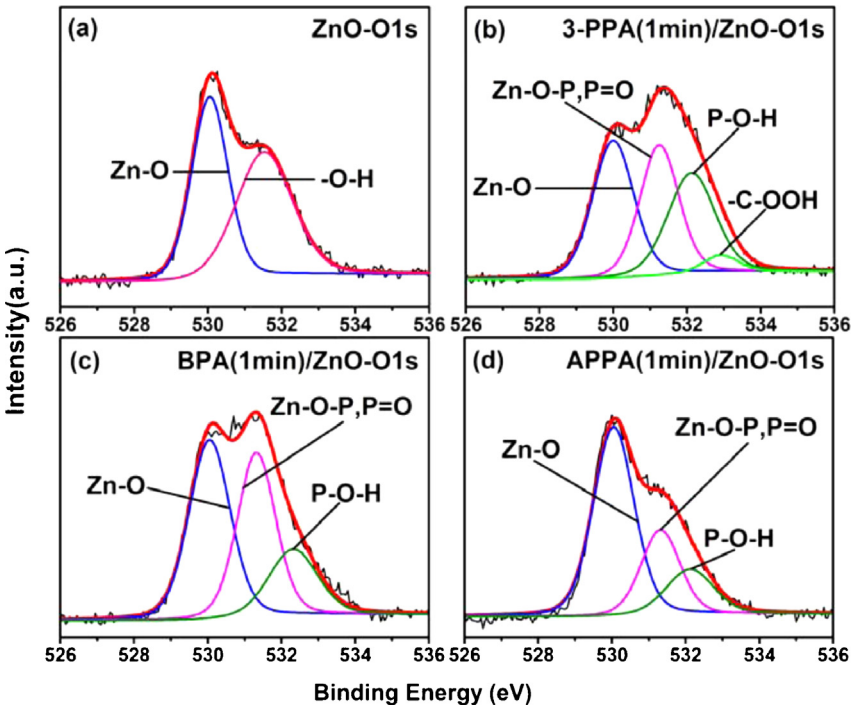

Fig. 4. The O1s XPS spectra of ZnO NRs (a), 3-PPA(1 min)/ZnO (b), BPA(1 min)/ZnO (c) and APPA(1 min)/ZnO(d).

NRs were characterized by TEM technique. Fig. 3(a), (c), (e) and (g) present the TEM images of ZnO NRs, 3-PPA(1 min)/ZnO, BPA (1 min)/ZnO and APPA(1 min)/ZnO, respectively, which clearly shows that the average diameter of four samples is ~150 nm. In comparison with pure ZnO NRs, the surfaces of three SAMs(1 min)/ZnO samples turn rough and some amorphous state of matter obviously attaches on the surface of ZnO NRs. Fig. 3(b), (d), (f) and (h) show the HRTEM images of ZnO NRs, 3-PPA(1 min)/ZnO, BPA (1 min)/ZnO and APPA(1 min)/ZnO, respectively. The well-resolved lattice fringe spacing for these samples can be distinguished to be 0.26 nm, corresponding to the typical wurtzite structure of ZnO. Moreover, from Fig. 3(d), (f) and (h), we can evaluate that the thickness of those thin amorphous layer is ~5 nm, ~4 nm and ~3 nm corresponding to 3-PPA(1 min)/ZnO, BPA(1 min)/ZnO and APPA(1 min)/ZnO samples, respectively. Here we would like to mention that, to prepare the sample for TEM measurement, we utilized the blade to scrape the ZnO and SAMs(1 min)/ZnO nanorods off the ITO surface. They were collected on the copper screen, then we dropped a few drops of ethanol on the copper screen to remove the contaminations and dried them at room temperature. Since the amorphous layer did not appear on the surface of pure ZnO nanorods as shown in Fig. 2(b), we can deduce that these thin amorphous layers on the surface of SAMs(1 min)/ZnO samples are originated from SAMs.

To further testify the TEM results, we use XPS technique to investigate the surface chemical composition of ZnO NRs, 3-PPA (1 min)/ZnO, BPA(1 min)/ZnO and APPA(1 min)/ZnO. Fig. 4 shows the O1s XPS spectra of ZnO, 3-PPA(1 min)/ZnO, BPA(1 min)/ZnO and APPA(1 min)/ZnO, respectively. From Fig. 4(a), we can see that two peaks of O1s are needed to obtain a good fitting for the O1s XPS spectrum of ZnO NRs by the XPSpeak curve-fitting procedure. The peak located at 530.05 eV can be assigned to the oxygen from zinc oxide(Zn-O). [34] The peak located at 531.53 eV can be assigned to the —O—H from the chemisorbed oxygen caused by surface hydroxyl [25]. In Fig. 4(b), the deconvolutions of four fitting curves indicate four oxygen species exist in 3-PPA(1 min)/ZnO. The peak located at 530.05 eV can be assigned to the oxygen from zinc oxide (Zn-O). The peaks located at 531.25 eV and 532.12 eV are ascribed to the oxygen in the phosphate group of P=O and P—O—H, respectively [35]. The peaks located at 532.92 eV is originated from the oxygen in the carboxyl group (—COOH) [35]. Referring to the results of Fig. 4(b), we can determine that three peaks in Fig. 4(c) and Fig. 4(d) of BPA(1 min)/ZnO and APPA(1 min)/ZnO are originated from Zn-O, (Zn—O—P, P=O) and P—O—H, respectively. According to the molecule formula of three SAMs shown in Fig. 1, XPS results indicate that the surface of ZnO NRs have been successfully modified by 3-PPA, BPA and APPA, respectively.

To further prove the origination of thin amorphous layer on the surface of ZnO NRs in 3-PPA(1 min)/ZnO, BPA(1 min)/ZnO and APPA (1 min)/ZnO samples, we performed the FT-IR measurements. To make a reference, the 3-PPA, BPA and APPA powders were characterized by transmission FT-IR technique. Fig. 5 demonstrates the transmission FT-IR spectra of 3-PPA, BPA and APPA powders and reflectance FT-IR spectra of ZnO NRs, 3-PPA(1 min)/ZnO, BPA (1 min)/ZnO and APPA(1 min)/ZnO. In the FT-IR spectrum of ZnO NRs shown in Fig. 5(a), the peak at 2850~2966 cm^{-1} is known as the C—H stretching vibration ν(C—H), the peak at 3060~3826 cm^{-1} is identical to the presence of hydroxyl stretching vibration ν(O—H) [36]. In the FT-IR spectrum of pure 3-PPA powder shown in Fig. 5(b), the peaks at 2969 cm^{-1} is identical to the presence of hydroxyl stretching vibration ν(O—H), which is originated from 3-PPA according to its molecule formula. In the carbonyl stretching region, the strong peak located at 1716 cm^{-1} is due to the C=O stretch of the carboxylic group [36] and the peak occurring at 1267 cm^{-1} is ascribed to the C—O stretching in carboxylic groups [37]. The two characteristic peaks in the region of 900 cm^{-1}~1050 cm^{-1} are originated from P—O—H group [36]. The band at 1207 cm^{-1} is related to P=O stretching [36]. The position of ν(O—H), C=O, C—O and P—O—H characteristic peaks in the FT-IR spectrum of 3-PPA(1 min)/ZnO sample can be well matched with that of pure 3-PPA powder as shown in Fig. 5(c). But the intensities of P—O—H and P=O stretching characteristic peaks turn much

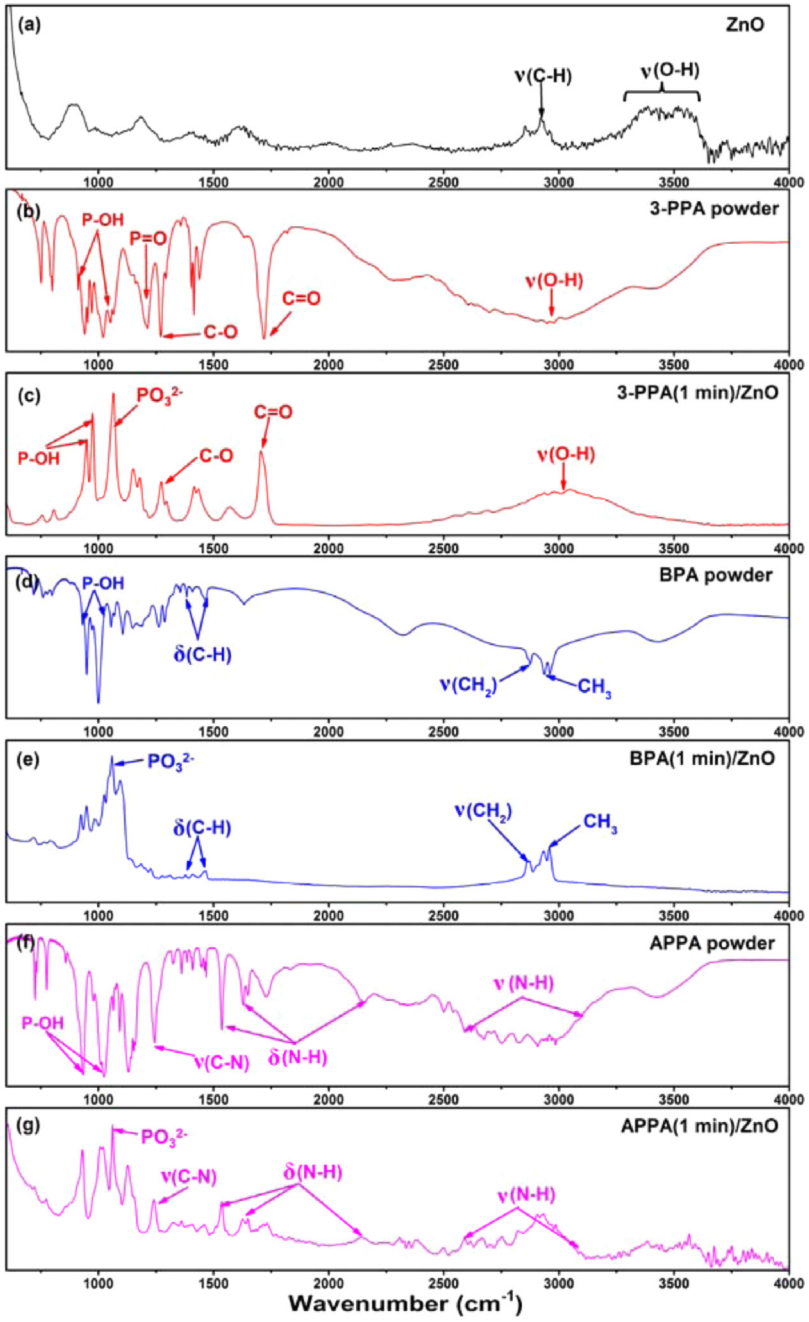

Fig. 5. FT-IR spectra of ZnO NRs (a), 3-PPA powder (b), 3-PPA(1 min)/ZnO (c), BPA powder (d), BPA(1 min)/ZnO (e), APPA powder (f) and APPA(1 min)/ZnO (g). The pure SAMs powders sample was characterized by transmission FT-IR technique. The ZnO NRs and SAMs/ZnO samples on the ITO substrates were directly tested by FT-IR under reflectance configuration mode.

lower. Meanwhile, a new strong peak around 1060 cm^{-1} appears. It is typically assigned to the stretches of PO_3^{2-} group anchored to the surface through a multidentate bonding, which involves both P—O and P=O terminations [38,39]. These data can confirm that 3-PPA molecule is bonded to the surface through the phosphonic group. Once the 3-PPA is adsorbed by a single condensation, the phosphonic group can interact with the surface by means of a further condensation process. In this case, the interaction between 3-PPA and ZnO surface consists of a double condensation between the two P —O —H terminations and the surface hydroxyl groups on two Zn atoms, leading to a bridging bidentate coordination bonding [35]. Similarly, in FT-IR spectra of BPA powder as shown in Fig. 5(d), the peaks in the region of 900 cm^{-1}~1050 cm^{-1} range are originated from P—O—H group. The peak at 2930 cm^{-1} and 2960 cm^{-1} are known as the $-CH_3$ asymmetric and symmetric stretches [35]. The peak at 2869 cm^{-1} can be assigned to the $-CH_2$ stretching vibration $\nu(CH_2)$. The peaks at 1382 cm^{-1} and 1462 cm^{-1} are identical to the presence of C—H bending vibration δ(C—H) [40]. In comparison to Fig. 5(d), the absence of P=O stretching, weaker intensity of P—O—H characteristic peaks and appearance of strong PO_3^{2-} peak at 1058 cm^{-1} in the FT-IR spectrum of BPA (1 min)/ZnO sample shown in Fig. 5(e) confirm that BPA molecule is bonded to the surface through the phosphonic group as well. In a similar way, the FTIR spectra of APPA powder and APPA(1 min)/ZnO samples are illustrated in Fig. 5(f) and Fig. 5(g). The peaks in the region of 900 cm^{-1}~1050 cm^{-1} range are originated from P—O—H group. The peak at 2600 cm^{-1}~3100 cm^{-1} is ascribed to the N—H stretching vibration ν(N—H). The peak located around 1242 cm^{-1}

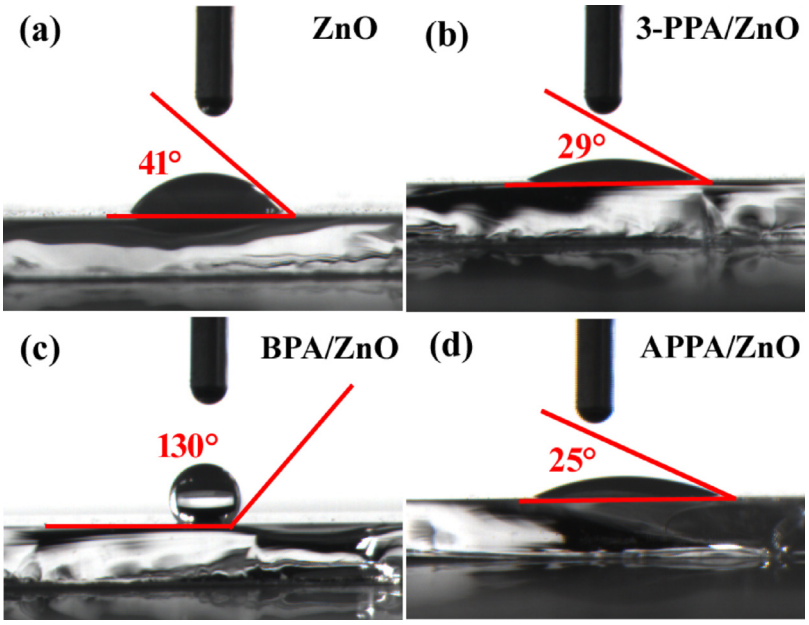

Fig. 6. Water contact angle of ZnO NRs (a), 3-PPA(1 min)/ZnO (b), BPA(1 min)/ZnO (c) and APPA(1 min)/ZnO (d).

can be attributed to the C—N stretching vibration ν(C—N). The three characteristic peaks in the region of 1536 cm^{-1}~1651 cm^{-1} and 2151 cm^{-1} are originated from the N—H bending vibration δ(N—H). As compared to Fig. 5(f), we can find that the intensities of P=O and P—O—H characteristic peaks obviously turn weak and PO_3^{2-} peak appears. These phenomena indicate that BPA molecule bonded to the surface through the phosphonic group too. According to the above discussion, we can deduce that three kinds of SAMs molecules attach on the ZnO NRs surface mainly through the phosphate groups.

Wettability is another effective way to distinguish the surface variation. In our case, the wettability was studied by measuring the contact angle of all samples with water. Generally, if the water contact angle is smaller than 90°, the solid surface is considered hydrophilic and if the water contact angle is larger than 90°, the solid surface is considered hydrophobic [41]. Fig. 6 shows the water contact angles of ZnO NRs and three kinds of SAMs/ZnO NRs. From the Fig. 6(a), we can see the water contact angle of ZnO NRs without any SAMs is 41°. For 3-PPA(1 min)/ZnO and APPA(1 min)/ZnO, the water contact angles are decreased to 29° (Fig. 6(b)) and 25° (Fig. 6(d)), respectively. But for BPA(1 min)/ZnO, the water contact angle is increased to 130° (Fig. 6(c)). Since three kinds of SAMs attached on the surface of ZnO NRs mainly by the phosphate

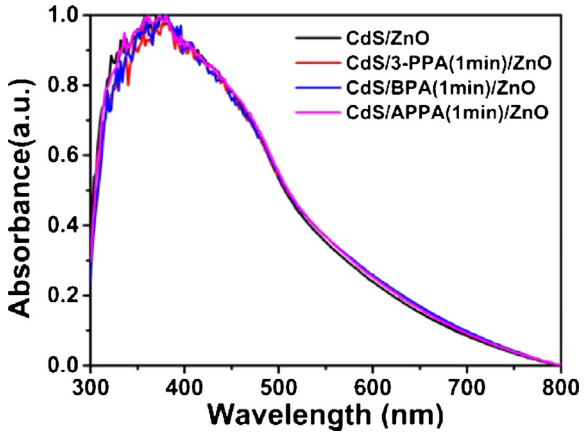

Fig. 7. UV–vis absorption spectra of CdS/ZnO and CdS/SAMs(1 min)/ZnO.

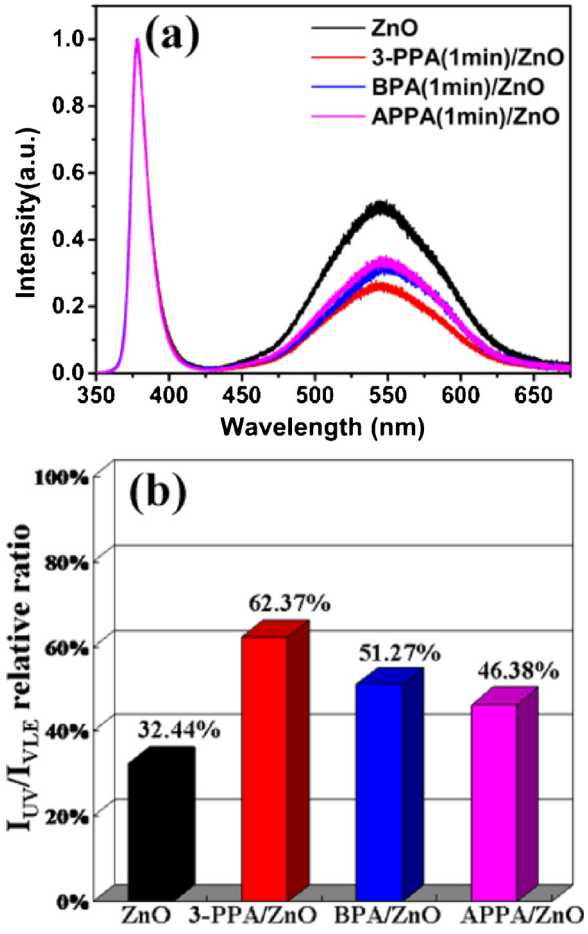

Fig. 8. (a) Room temperature PL spectra of ZnO NRs, 3-PPA(1 min)/ZnO, BPA(1 min)/ZnO and APPA(1 min)/ZnO; (b) Relative intensity ratio of UV emission to visible light emission (I_{UV}/I_{VLE}) of all samples.

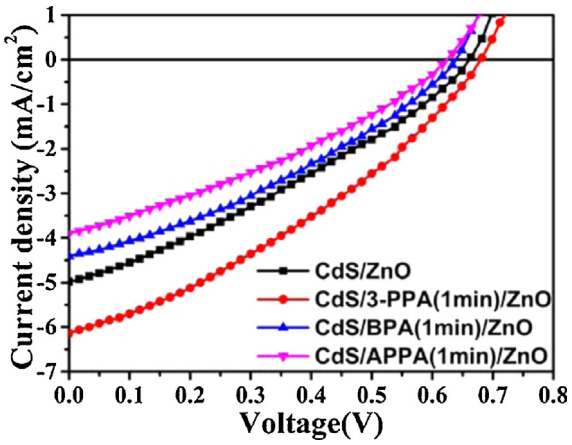

Fig. 9. I–V characteristics of CdS/ZnO NRs, CdS/3-PPA(1 min)/ZnO, CdS/BPA(1 min)/ZnO and CdS/APPA(1 min)/ZnO QDSSCs.

Table 1
Photovoltaic parameters obtained from the I–V curves of QDSSCs with depositing different kinds of SAMs: 3-PPA, BPA and APPA.

Photoelectrodes	Jsc (mA/cm^2)	Voc (V)	FF	η (%)
CdS/ZnO	4.98	0.661	0.307	1.01
CdS/3-PPA(1min)/ZnO	6.15	0.680	0.337	1.41
CdS/BPA(1min)/ZnO	4.45	0.641	0.333	0.95
CdS/APPA(1min)/ZnO	3.89	0.624	0.329	0.80

head groups, such difference in water contact angles should be determined by their tailgroups. We know that the tailgroups of 3-PPA and APPA are —COOH and —NH2, respectively, which are hydrophilic groups, so the surfaces of the ZnO NRs become more hydrophilic after the treatment. On the contrary, the tailgroups of BPA is —CH_3, which is a kind of hydrophobic groups, so the surface of ZnO NRs after modification turns more hydrophobic. According to the water contact angle results, we can further confirm the SAMs were deposited on the ZnO NRs surface.

Fig. 7 shows the optical absorption spectra of CdS/ZnO and CdS/SAMs/ZnO phtoanodes. We can see that the intensities of optical absorption do not obviously change after depositing different SAMs, indicating that the deposition of SAMs dose not significantly influence the uptake of CdS QDs on the ZnO surfaces. The room temperature photoluminescence (PL) spectra of ZnO NRs, 3-PPA (1 min)/ZnO, BPA(1 min)/ZnO and APPA(1 min)/ZnO are illustrated in Fig. 8(a). All the spectra consist of two peaks. One is a UV emission peak located at 378 nm; the other is a broad visible light emission (VLE) band in the range of 435∼640 nm. The UV emission band is ascribed to a near band edge transition of ZnO, which is originated from the recombination of free excitons through an exciton-exciton collision process [42]. The VLE peak is related to deep-level defects in the ZnO crystal, such as vacancies and interstitials of zinc and oxygen [43,44]. To see it clearly, all PL spectra are normalized to the UV emission of ZnO NRs. Obviously, the VLE intensity reduces after depositing three kinds of SAMs, indicating that the defects at the surface of ZnO NRs have been strongly suppressed due to the SAMs modification. It is well known that the surfaces of ZnO NRs grown with CBD method are prone to absorb various kinds of functional groups. According to the chemical reaction in the solution, these functional groups should be related to the elements such as carbon, nitrogen, and hydrogen [45]. After depositing SAMs, the ruptured Zn—O bond on the ZnO NRs surfaces are combined with —POOH of SAMs, which passivates a part of surface defects in ZnO NRs.

Fig. 8(b) summarizes the relative intensity ratio of UV emission to VLE band (I_{UV}/I_{VLE}) for ZnO NRs, 3-PPA(1 min)/ZnO, BPA(1 min)/ZnO and APPA(1 min)/ZnO. We can see that the I_{UV}/I_{VLE} values of 3-PPA(1 min)/ZnO, BPA(1 min)/ZnO and APPA(1 min)/ZnO are larger than that of as-grown ZnO. It indicates that the surface defects have been reduced after depositing different kinds of SAMs

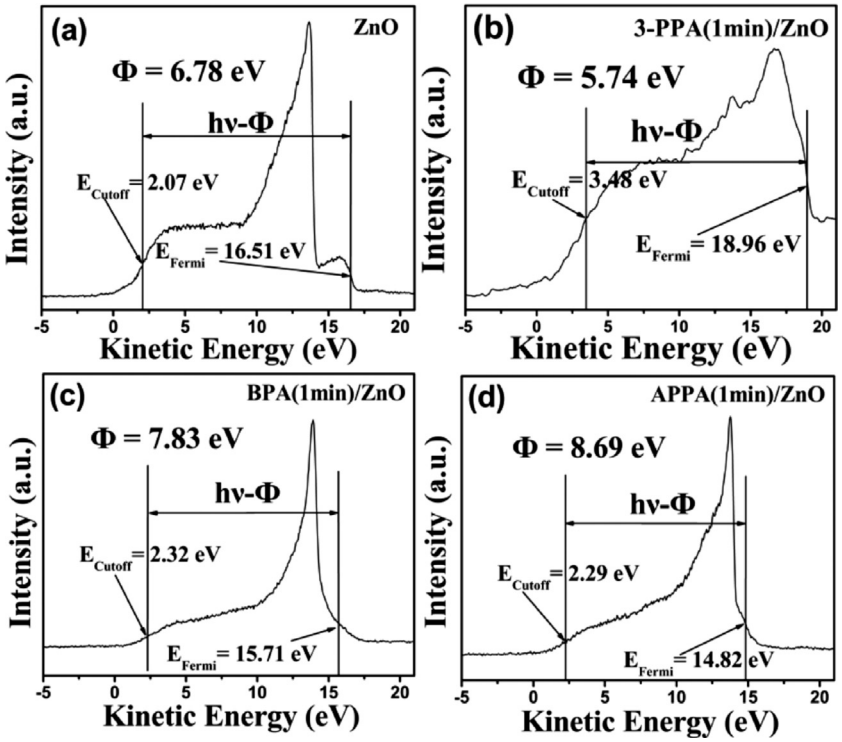

Fig. 10. The typical He I (hν = 21.22 eV) UPS spectrum of ZnO NRs (a), 3-PPA(1 min)/ZnO (b), BPA(1 min)/ZnO (c) and APPA(1 min)/ZnO (d) taken with −8 V bias applied to the sample. Also shown is inelastic cutoff (E_{Cutoff}) and Fermi edge (E_{Fermi}). The relation between spectrum width hν, and work function Φ is illustrated.

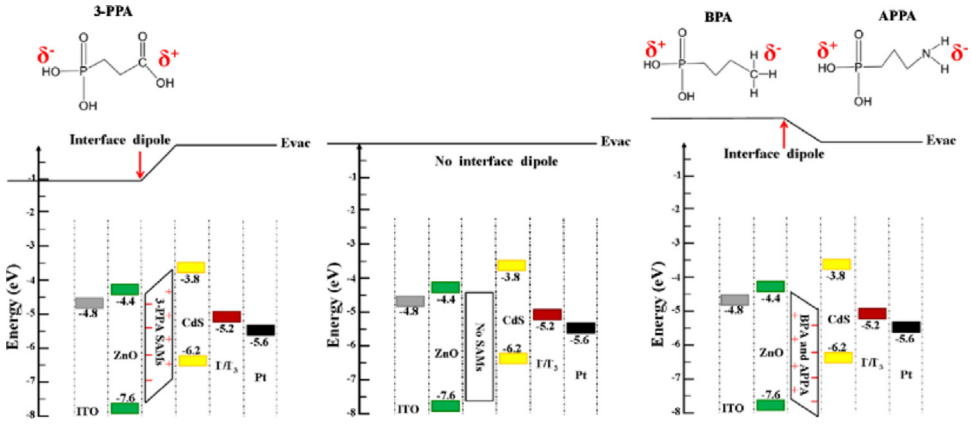

Fig. 11. Illustration of schematic energy diagrams of ZnO NRs, 3-PPA(1 min)/ZnO, BPA(1 min)/ZnO and APPA(1 min)/ZnO solar cells. The interface dipole of SAMs treated ZnO directed toward or away from the surface. No interface dipole for untreated ZnO.

on ZnO NRs array. Moreover, the 3-PPA(1 min)/ZnO exhibits the largest I_{UV}/I_{VLE} value, which means the 3-PPA exhibits the best effect for suppressing the surface defects of ZnO. Therefore, we prospect that maybe we can get the best performance in the solar cell with 3-PPA(1 min)/ZnO as photoanode.

The I–V characteristics of all solar cells were carried out under 1.5AM light illumination. The I–V curves for ZnO NRs, 3-PPA (1 min)/ZnO, BPA(1 min)/ZnO and APPA(1 min)/ZnO QDSSCs are displayed in Fig. 9. The corresponding performance parameters for each cell are calculated and listed in Table 1, including the short-circuit current density (Isc), the open-circuit voltage (Voc), the fill factor (FF), and the photovoltaic conversion efficiency (η). According to the results in Table 1, the best photovoltaic performance comes from the CdS/3-PPA(1 min)/ZnO solar cell, which owns a higher η of 1.41%, Isc of 6.15 mA/cm^2, Voc of 0.680 V and FF of 0.337. Compared to the ZnO solar cell, the η of 3-PPA (1 min)/ZnO solar cell significantly increases from 1.01% to 1.41%. This up to ~40% enhancement of η should be attributed to the increase of both Isc from 4.98 mA/cm^2 to 6.15 mA/cm^2 and FF from 0.307 to 0.337. But for the BPA(1 min)/ZnO and APPA(1 min)/ZnO solar cell, we can find that the η decreases to 0.95% and 0.80%, the Isc decreases to 4.45 mA/cm^2 and 3.89 mA/cm^2, and the Voc decreases to 0.641 and 0.624.

Since the Voc value is mainly depending on the band offset between ZnO (SAMs/ZnO) and CdS QDs in our case. Hence, we utilized UPS technique to investigate the variation of surface work function of SAMs/ZnO in comparison with pure ZnO. Fig. 10 shows the typical He I UPS spectra for ZnO NRs, 3-PPA(1 min)/ZnO, BPA (1 min)/ZnO and APPA(1 min)/ZnO in kinetic energy scale. According to Einstein photoelectric law as follows:

$$h\nu - \Phi = F_{Fermi} - E_{Cutoff} \text{or} \Phi = h\nu + E_{Cutoff} - F_{Fermi} \quad (1)$$

The figure also illustrates the relation between the width of the spectrum, work function Φ and photon energy $h\nu$. From Fig. 10(a), we can see that the E_{Cutoff} and E_{Fermi} of ZnO NRs are 2.07 eV and 16.51 eV, respectively. The work function of ZnO NRs can be calculated to be 6.78 eV according to the formula (1). Similarly, the work function of 3-PPA(1 min)/ZnO, BPA(1 min)/ZnO and APPA (1 min)/ZnO can be determined to be 5.74 eV, 7.83 eV and 8.69 eV, respectively, as shown in Fig. 10(b)–(d). Compared to pure ZnO, the Φ of 3-PPA/ZnO is decreased by 1.04 eV, but the Φ of BPA/ZnO and APPA/ZnO is increased by 1.05 eV and 1.91 eV, respectively.

Usually, the work function difference is proportionally depending on the surface potential difference. In our case, the change in the ZnO surface potential varies linearly with the electron affinity of the tailgroup of three SAMs. The dipole moments of these tailgroups reflect their electron-withdrawing and -donating power. The strong electron-donating power tailgroup reduces the surface potential and work function of the semiconductor [46,47]. Since the tailgroup of —COOH is electron-withdrawing groups, the direction of the dipole moment of 3-PPA is from tailgroup to headgroup, which means the interface dipole of 3-PPA/ZnO is directed toward the ZnO surface. Thus, the effective work function of ZnO modified with 3-PPA is smaller than that of ZnO NRs, which is consistent with the UPS results. However, for BPA and APPA, the tailgroups of $-CH_3$ and $-NH_2$ are the electron-donating groups, so that the direction of the dipole moment is from headgroup to tailgroup. Thus, their directions of interface dipole are exactly reverse to that of 3-PPA so that their work functions are correspondingly larger than that of ZnO NRs, which is consistent with the UPS results as well.

Based on the above discussion, we drew the schematic energy diagrams of ZnO NRs, 3-PPA(1 min)/ZnO, BPA(1 min)/ZnO and APPA(1 min)/ZnO solar cells in Fig. 11. We can see that the interface dipole of 3-PPA/ZnO is directed toward the ZnO surface and the work function of 3-PPA(1 min)/ZnO decreases after 3-PPA modification, so that a energy barrier has been formed between CdS and ZnO, which is very efficient on retarding the back transfer of electrons. In addition, the 3-PPA acted as a SAMs layer can suppress the electron-hole recombination process due to its passivation on the surface defects, which finally results in the enhancement of conversion efficiency of solar cells. But for the BPA and APPA, the work function of BPA(1 min)/ZnO and APPA(1 min)/ZnO are increased due to the formation of unfavorable interface dipole, so that the BPA and APPA SAMs hinder the transmission of photoelectrons from CdS to ZnO and result in the lower photovoltaic conversion efficiency.

4. Conclusions

In this work, we chose 3-PPA, BPA and APPA as SAMs layer to modify the ZnO nanorods photoanodes and revealed their influence mechanism on the photovoltaic performance of QDSSCs. The results indicated that the deposition of SAMs layer can not only passivate the surface defects of ZnO, but also tune the work function of ZnO surface. In particular, the 3-PPA modification exhibits the best passivation effect and makes the surface work function of ZnO decreases by 1.04 eV to realize a better band alignment due to its electron-withdrawing tailgroup, which results

in an enhancement in photovoltaic conversion efficiency of solar cells. Our work provides an alternative approach to improve the performances of QDSSCs by the interface modification with SAMs in a simple operation process, which will prompt other researchers to further design and optimize the SAMs to obtain even higher photovoltaic performance of QDSSCs.

Acknowledgements

The authors would like to acknowledge financial support for this work from National Nature Science Foundation of China (Grant Nos. 11204104,61475063, and 11254001), Program for New Century Excellent Talents in University (No. NCET-13-0824), Program for the Development of Science and Technology of Jilin province (Item Nos. 201205078 and 20110415), the Twentieth Five-Year Program for Science and Technology of Education Department of Jilin Province (Item No. 20140147), National Programs for High Technology Research and Development of China (863) (Item No. 2013AA032202), Program for the Master Students' scientific and Innovative Research of Jilin Normal University (Item No. 2013022).

Appendix A. Supplementary data

Supplementary data associated with this article can be found, in the online version, at http://dx.doi.org/10.1016/j.electacta.2015.02.190.

References

[1] S. Mathew, A. Yella, P. Gao, R. Humphry-Baker, B.F.E. Curchod, N. shari-Astani, I. Tavernelli, U. Rothlisberger, Md K. Nazeeruddin, M. Grätzel, Dye-sensitized solar cells with 13% efficiency achieved through the molecular engineering of porphyrin sensitizers, Nature Chemistry 6 (2014) 242.
[2] K.E. Roelofs, T.P. Brennan, J.C. Dominguez, C.D. Bailie, G.Y. Margulis, E.T. Hoke, M.D. McGehee, S.F. Bent, Effect of Al_2O_3 Recombination Barrier Layers Deposited by Atomic Layer Deposition in Solid-State CdS Quantum Dot-Sensitized Solar Cells, J. Phys. Chem. C 117 (2013) 5584.
[3] M.S. Lim, K. Feng, X.Q. Chen, N.Q. Wu, A. Raman, J. Nightingale, E.S. Gawalt, D. Korakakis, L.A. Hornak, A.T. Timperman, Adsorption and Desorption of Stearic Acid Self-Assembled Monolayers on Aluminum Oxide, Langmuir 23 (2007) 2444.
[4] D.L. Allara, R.G. Nuzzo, Spontaneously Organized Molecular Assemblies.1. Formation Dynamics, and Physical Properties of n-Alkanoic Acids Adsorbed from Solution on an Oxidized Aluminum Surface, Langmuir 1 (1985) 45.
[5] Y.T. Tao, Structural Comparison of Self-Assembled Monolayers of n-Alkanoic Acids on the Surfaces of Silver, Copper, and Aluminum, J. Am. Chem. Soc. 115 (1993) 4350.
[6] H.I. Kim, T. Koini, T.R. Lee, S.S. Perry, Systematic Studies of the Frictional Properties of Fluorinated Monolayers with Atomic Force Microscopy: Comparison of CF3- and CH3-Terminated Films, Langmuir 13 (1997) 7192.
[7] H.I. Kim, M. Graupe, O. Oloba, T. Koini, S. Imaduddin, T.R. Lee, S.S. Perry, Molecularly Specific Studies of the Frictional Properties of Monolayer Films: ASystematic Comparison of CF3-, (CH3) 2CH-, and CH3-Terminated Films, Langmuir 15 (1999) 3179.
[8] S. Lee, Y.-S. Shon, J.R. Colorado, R.L. Guenard, T.R. Lee, S.S. Perry, The Influence of Packing Densities and Surface Order on the Frictional Properties of Alkanethiol Self-Assembled Monolayers (SAMs) on Gold: A Comparison of SAMs Derived from Normal and Spiroalkanedithiols, Langmuir 16 (2000) 2220.
[9] H.I. Kim, T. Koini, T.R. Lee, S.S. Perry, Molecular contribution to the frictional properties of fluorinated self-assembled monolayers, Tribol. Lett. 4 (1998) 137.
[10] C.G. Allen, D.J. Baker, J.M. Albin, H.E. Oertli, D.T. Gillaspie, D.C. Olson, T.E. Furtak, R.T. Collins, Surface Modification of ZnO Using Triethoxysilane-Based Molecules, Langmuir 24 (2008) 13393.
[11] K. Ozawa, T. Hasegawa, K. Edamoto, K. Takahashi, M. Kamada, Adsorption State and Molecular Orientation of Ammonia on ZnO(1010) Studied by Photoelectron Spectroscopy and near-Edge X-ray Absorption Fine Structure Spectroscopy, J. Phys. Chem. B 106 (2002) 9380.
[12] J.B.L. Martins, E. Longo, O.D.R. Salmon, V.A.A. Espinoza, C.A. Taft, The interaction of H_2 CO, CO_2, H_2O and NH_3 on ZnO surfaces: an Oniom Study, Chem. Phys. Lett. 400 (2004) 481.
[13] L. Thomsen, B. Watts, P.C. Dastoor, A NEXAFS orientation study of γ-aminopropyltriethoxysilane on zinc oxide surfaces, Surf. Interface Anal. 38 (2006) 1139.
[14] C.L. Rhodes, S. Lappi, D. Fischer, S. Sambasivan, J. Genzer, S. Franzen, Characterization of Monolayer Formation on Aluminum-Doped Zinc Oxide Thin Films, Langmuir 24 (2008) 433.
[15] P.W. Sadik, S.J. Pearton, D.P. Norton, E. Lambers, F. Ren, Functionalizing Zn- and O-terminated ZnO with thiols, J. Appl. Phys. 101 (2007) 104514.
[16] C. Nogues, P. Lang, Self-Assembled Alkanethiol Monolayers on a Zn Substrate: Structure and Organization, Langmuir 23 (2007) 8385.
[17] H.L. Yip, S.K. Hau, N.S. Baek, A.K.Y. Jen, Self-assembled monolayer modified ZnO/metal bilayer cathodes for polymer/fullerene bulk-heterojunction solar cells, Appl. Phys. Lett. 92 (2008) 193313.
[18] Y.S. Chen, C. Li, Z.H. Zeng, W.B. Wang, X.S. Wang, B.W. Zhang, Efficient electron injection due to a special adsorbing group's combination of carboxyl and hydroxyl: dye-sensitized solar cells based on new hemicyanine dyes, J. Mater. Chem. 15 (2005) 1654.
[19] A. Domínguez, N.H. Moreira, G. Dolgonos, T. Frauenheim, A.L. da Rosa, Glycine Adsorption on (1010) ZnO Surfaces, J. Phys. Chem. C 115 (2011) 6491.
[20] F. Labat, I. Ciofini, H.P. Hratchian, M. Frisch, K. Raghavachari, C. Adamo, First Principles Modeling of Eosin-Loaded ZnO Films: A Step toward the Understanding of Dye-Sensitized Solar Cell Performances, J. Am. Chem. Soc. 131 (2009) 14290.
[21] N.H. Moreira, R.A.L. da, T. Frauenheim, Covalent functionalization of ZnO surfaces: A density functional tight binding study, Appl. Phys. Lett. 94 (2009) 193109.
[22] P. Persson, S. Lunell, L. Ojamae, Quantum chemical prediction of the adsorption conformations and dynamics at HCOOH-covered ZnO(1010) surfaces, Int. J. Quantum Chem. 89 (2002) 172.
[23] X. Tian, J. Xu, W. Xie, Controllable Modulation of the Electronic Structure of ZnO(1010) Surface by Carboxylic Acids, J. Phys. Chem. C 114 (2010) 3973.
[24] P.J. Hotchkiss, M. Malicki, A.J. Giordano, N.R. Armstrong, S.R. Marder, Characterization of phosphonic acid binding to zinc oxide, J. Mater. Chem. 21 (2011) 3107.
[25] B.B. Zhang, T. Kong, W.Z. Xu, R.G. Su, Y.H. Gao, G.S. Cheng, Surface Functionalization of Zinc Oxide by Carboxyalkylphosphonic Acid Self-Assembled Monolayers, Langmuir 26 (2010) 4514.
[26] Y. Paukku, A. Michalkova, J. Leszczynski, Quantum-Chemical Comprehensive Study of the Organophosphorus Compounds Adsorption on Zinc Oxide Surfaces, J. Phys. Chem. C 113 (2009) 1474.
[27] C. Wood, H. Li, P. Winget, J.-L. Brédas, Binding Modes of Fluorinated Benzylphosphonic Acids on the Polar ZnO Surface and Impact on Work Function, J. Phys. Chem. C 116 (2012) 19125.
[28] C.L. Perkins, Molecular Anchors for Self-Assembled Monolayers on ZnO: A Direct Comparison of the Thiol and Phosphonic Acid Moieties, J. Phys. Chem. C 113 (2009) 18276.
[29] L.L. Yang, Q.X. Zhao, M. Willander, Size-controlled growth of well-aligned ZnO nanorod arrays with two-step chemical bath deposition method, J. Alloy. Compd. 469 (2009) 623.
[30] L.L. Yang, Q.X. Zhao, M. Willander, J.H. Yang, Effective way to control the size of well-aligned ZnO nanorod arrays withtwo-step chemical bath deposition, J. Cryst. Growth 311 (2009) 1046.
[31] Q.X. Zhao, L.L. Yang, M. Willander, B.E. Sernelius, P.O. Holtz, Surface recombination in ZnO nanorods grown by chemical bath deposition, J. Appl. Phys. 104 (2008) 073526.
[32] H.M. Pathan, C.D. Lokhande, Deposition of Metal Chalcogenide Thin Films by Successive Ionic Layer Adsorption and Reaction (SILAR) Method, Bull. Mater. Sci. 27 (2004) 85–111.
[33] D.D. Wang, J.H. Yang, G.Z. Xing, L.L. Yang, J.H. Lang, M. Gao, B. Yao, T. Wu, Abnormal blueshift of UV emission in single-crystalline ZnO nanowires, J. Lumin. 129 (2009) 996.
[34] L.L. Yang, Q.X. Zhao, M. Willander, X.J. Liu, M. Fahlman, J.H. Yang, Origin of the surface recombination centers in ZnO nanorods arrays by X-ray photoelectron spectroscopy, Appl. Surf. Sci. 256 (2010) 3592.
[35] Y.E. Ha, M.Y. Jo, J. Park, Y.-C. Kang, S.I. Yoo, J.H. Kim, Inverted Type Polymer Solar Cells with Self-Assembled Monolayer Treated ZnO, J. Phys. Chem. C 117 (2013) 2646.
[36] E. Smecca, A. Motta, M.E. Fragalà, Y. Aleeva, G.G. Condorelli, Spectroscopic and Theoretical Study of the Grafting Modes of Phosphonic Acids on ZnO Nanorods, J. Phys. Chem. C 117 (2013) 5364.
[37] H. Liu, Q. Gao, P. Dai, J. Zhang, C. l. Zhang, N. Bao, Preparation and characterization of activated carbon from lotus stalk with guanidine phosphate activation: Sorption of Cd(II), J. Anal. Appl. Pyrol. 102 (2013) 7.
[38] U. Dembereldorj, E.-O. Ganbold, J.-H. Seo, S.Y. Lee, S.I. Yang, S.-W. Joo, Conformational changes of proteins adsorbed onto ZnO nanoparticle surfaces investigated by concentration-dependent infrared spectroscopy, Vib. Spectrosc. 59 (2012) 23.
[39] R. Luschtinetz, G. Seifert, E. Jaehne, H.-J.P. Adler, Infrared Spectra of Alkylphosphonic Acid Bound to Aluminium Surfaces, Macromol. Symp. 254 (2007) 248.
[40] J. Zhang, J.Y. Zhang, Surfactant Inducing Phase Change of ZnO Nanorods to Low Friction, Tribol Lett 49 (2013) 77.
[41] S.A. Vanalakar, S.S. Mali, R.C. Pawar, N.L. Tarwal, A.V. Moholkar, J.H. Kim, P.S. Patil, Photoelectrochemical properties of CdS sensitized ZnO nanorod arrays: Effect of nanorod length, J. Appl. Phys. 112 (2012) 044302.
[42] Y.F. Sun, J.H. Yang, L.L. Yang, M. Gao, X.N. Shan, Z.Q. Zhang, M.B. Wei, Y. Liu, L.H. Fei, H. Song, Less contribution of nonradiative recombination in ZnO nailscompared with rods, Journal of Luminescence 134 (2013) 35.
[43] C. Ronning, P. Gao, X.Y. Ding, Z.L. Wang, D. Schwen, Manganese-doped ZnOnanobelts for spintronics, Applied Physics Letters 84 (2004) 783.

[44] P. Yang, H.Q. Yan, S. Mao, R. Russo, J. Johnson, R. Saykally, N. Morris, J. Pham, R. He, H.J. Choi, Controlled growth of ZnO nanowires and their optical properties, Advanced Functional Materials 12 (2002) 323.
[45] L.L. Yang, Z.Q. Zhang, J.H. Yang, Y.S. Yan, Y.F. Sun, J. Cao, M. Gao, M.B. Wei, J.H. Lang, F.Z. Liu, Z. Wang, Effect of tube depth on the photovoltaic performance of CdS quantum dots sensitized ZnO nanotubes solar cells, J. Alloy. Compd. 543 (2012) 58.
[46] Y.E. Ha, M.Y. Jo, J. Park, Y.-C. Kang, S.I. Yoo, J.H. Kim, Inverted Type Polymer Solar Cells with Self-Assembled Monolayer Treated ZnO, J. Phys. Chem. C 117 (2013) 2646.
[47] Y.E. Ha, M.Y. Jo, J. Park, Y.-C. Kang, S.-J. Moon, J.H. Kim, Effect of self-assembled monolayer treated ZnO as an electron transporting layer on the photovoltaic properties of inverted type polymer solar cells, Synthetic Metals 187 (2014) 113.